He*($2\,^3S$) penning ionization of H_2S. II. Formation of the $SH^+(A\,^3\Pi)$ and $H_2S^+(\tilde{A}\,^2A_1)$ ions

Ikuo Tokue[a] and Katsuyoshi Yamasaki
Department of Chemistry, Faculty of Science, Niigata University, Ikarashi, Niigata 950-2181, Japan

Shinkoh Nanbu
Research Center for Computational Science, Okazaki National Research Institutes, Myodaiji, Okazaki 444-8585, Japan

(Received 13 May 2003; accepted 26 June 2003)

Emissions in the 200–750 nm region produced by the collision of He*($2\,^3S$) with H_2S were studied under single-collision conditions. The hydrogen Balmer lines and the $SH^+(A\,^3\Pi-X\,^3\Sigma^-)$ and $H_2S^+(\tilde{A}\,^2A_1-\tilde{X}\,^2B_1)$ bands were assigned. The total emission cross section (σ_{em}) was evaluated to be $(1.7\pm0.3)\times10^{-20}$ m^2 at a collision energy of 150 meV. The σ_{em}s of the $SH^+(A-X)$ and $H_2S^+(\tilde{A}-\tilde{X})$ bands decreased with increase in the collision energy in the 115–200 meV range, indicating that attractive forces are effective for the incident channels with regard to the formation of these species. The rotational distribution of $SH^+(A\,^3\Pi,\nu'=0)$ is represented by a Boltzmann temperature of 870 ± 80 K. The $H_2S^+(\tilde{A}\,^2A_1-\tilde{X}\,^2B_1)$ emission, which was assigned for the first time in the Penning ionization of H_2S, primarily consists of the bending progressions. The internal populations of $H_2S^+(\tilde{A})$ were analyzed using the vibrational energies and Einstein's *A* coefficients calculated in this study. The details of the calculation and derived spectroscopic constants are reported in the accompanying paper, Paper I. The populations obtained for the bending vibration (ν_2') of $H_2S^+(\tilde{A})$ show an inverted distribution with a peak at $\nu_2'=3$. This distribution is shifted lower compared that with a peak at $\nu_2'=4-5$ observed by He*($2\,^3S$) Penning ionization electron spectroscopy and that with a peak at $\nu_2'=6-7$ predicted by the theoretical Franck–Condon factors for the $H_2S(\tilde{X})-H_2S^+(\tilde{A})$ ionization. The origin of the difference is discussed concerning the formation mechanism of $H_2S^+(\tilde{A}\,^2A_1)$. © *2003 American Institute of Physics.*
[DOI: 10.1063/1.1602064]

I. INTRODUCTION

When the He*($2\,^3S$: 19.82 eV) atom collides with hydrogen sulfide, Penning ionization is the primary decay channel. The Penning ionization of H_2S by the collision with He*($2\,^3S$) atoms was studied by electron spectroscopy (PIES) and optical spectroscopy (PIOS). In PIES, the $\tilde{X}\,^2B_1$, $\tilde{A}\,^2A_1$, and $\tilde{B}\,^2B_1$ states of the H_2S^+ ion were observed,[1–3] while the $SH^+(A\,^3\Pi-X\,^3\Sigma^-)$ emission and hydrogen Balmer lines were assigned in PIOS.[4,5] No emission from the parent ion was assigned in PIOS of H_2S. Nevertheless, emission from the parent ion may be expected from H_2S since the $H_2O^+(\tilde{A}\,^2A_1-\tilde{X}\,^2B_1)$ emission has been observed in the He*($2\,^3S$) Penning ionization of H_2O,[6] which is the isoelectronic molecule of H_2S. Moreover, very little is known about either the internal distribution of $SH^+(A\,^3\Pi)$ or its formation mechanism. Internal energy distributions and cross sections of the state-selected species, and their dependence on the collision energy are needed in order to study the reaction dynamics of the He*($2\,^3S$) Penning ionization of H_2S in detail. In this context, we observed the emission spectrum in the 200–750 nm region produced by the collision of He*($2\,^3S$) with H_2S. Based on these observation, the hydrogen Balmer lines and the $SH^+(A\,^3\Pi-X\,^3\Sigma^-)$ and $H_2S^+(\tilde{A}\,^2A_1-\tilde{X}\,^2B_1)$ bands were assigned. The emission cross sections (σ_{em}) of the $SH^+(A-X)$ and $H_2S^+(\tilde{A}-\tilde{X})$ bands were measured in the collision energy of the 115–200 meV range. The rotational and vibrational distributions of $SH^+(A)$ and $H_2S^+(\tilde{A})$ were then obtained from the analysis of the emission spectra.

This paper reports first the interaction between He*($2\,^3S$) and H_2S based on the experimental data and the model potentials calculated by *ab initio* methods. Next, the population analysis of the $SH^+(A-X)$ and $H_2S^+(\tilde{A}-\tilde{X})$ emissions are described. Several types of spectroscopic data such as vibrational and rotational energies, Franck–Condon factors (FCFs), the dependence of the electronic transition probability on the vibrational states, and Hönl–London factors are needed for the population analysis. In our preliminary analysis, the published data of vibrational energies and FCFs for the $H_2S^+(\tilde{A}-\tilde{X})$ band were found to be inadequate from both experimental and theoretical standpoints for analyzing the observed spectra. We have therefore obtained these data by theoretical calculations in the present study; the details are reported in Paper I. Finally, we discuss ionization processes from the internal distributions obtained for

[a]Author to whom correspondence should be addressed. Electronic mail: itok-pc@chem.sc.niigata-u.ac.jp

$SH^+(A)$ and $H_2S^+(\tilde{A})$ with the reported data. The main purpose of this paper is to describe the mechanism for the Penning ionization of H_2S based on the dependence of σ_{em} on the collision energy and the internal distribution of the product ions.

II. EXPERIMENT

The apparatus and experimental details concerning the fluorescence measurement have been reported previously.[7,8] In brief, He*($2\,^3S$,$2\,^1S$) atoms are produced with a nozzle discharge source[9] and skimmed into a collision chamber; the singlet component of the total He* flux was estimated to be approximately 10%. Target gases flowed out to the collision chamber, forming an effusive molecular beam through a multicapillary array. Under typical stable operating conditions, the discharge current was 10–30 mA, the voltage was 400–750 V, and the pressure of the residual gas at the collision chamber as measured by an ionization vacuum gauge was less than 2.7 mPa. The gases of H_2S (Takachiho, 99% in stated purity) and He (Nihon Sanso, 99.9999%) were used without further purification.

The velocity distribution of the He* beam measured by a time-of-flight method in the separate experiment was represented by a Gaussian function. The root-mean-square velocity (ν_A) of the He* beam was found to depend only on the discharge power at the beam source.[8] By using the relative velocity averaged over the velocities of He* atoms and the target molecules, the collision energy dependence of σ_{em} was obtained by converting the function of ν_A into that of the relative collision energy (E_R) with the relation between E_R and the reduced mass (μ) of the He+target system

$$E_R = \mu(\nu_A^2 + 3kT/m)/2, \tag{1}$$

where T is the temperature (300 K) and m is the mass of the target molecule. In the fluorescence measurement, we did not use the velocity-selected He* beam because of the weak fluorescence intensity. Thus, applying the fact that ν_A increases with the discharge power, we controlled the kinetic energy of the He* beam by varying the discharge power. The kinetic energy distribution of the He* beam was estimated to be 40 meV half width half maximum at $E_R = 120$ meV and 80 meV at 200 meV. The fluorescence resulting from the collision of He*($2\,^3S$) with H_2S was observed in a direction perpendicular to both the molecular and He* beams. The fluorescence focused on the entrance slit of a SPEX 1704 monochromator was detected by a charge coupled device (CCD) detector (PI, LN/CCD1100PB) for measurement of the high-resolution spectrum by or Hamamatsu R585 and R649 photomultipliers for other measurements. The σ_{em} for the fluorescence produced by the collision of He*($2\,^3S$) was evaluated by comparing its emission intensity with that of the $N_2^+(B\,^2\Sigma_u^+ - X\,^2\Sigma_g^+)$ band produced by the following Penning ionization:

$$\mathrm{He}(2\,^3S) + \mathrm{N_2} \rightarrow \mathrm{N_2^+}(B\,^2\Sigma_u^+) + \mathrm{He} + e. \tag{2}$$

We adopted a σ_{em} value of $(3.2 \pm 0.3) \times 10^{-20}$ m^2 for reaction (2) at an E_R of 140 meV; this value was estimated from Fig. 5 in Ref. 10. The total emission intensity of the $N_2^+(B-X)$ system was derived from the intensities of the 0–0 and 1–0 bands by using the scaling factors calculated by Comes and Speier.[11] The density and spatial distribution of N_2 and the target molecules at the collision region were calibrated, and the relative sensitivity of the total photon-detection system was calibrated with a deuterium lamp in the 200–310 nm range and with a halogen lamp in the 310–750 nm range.

III. THEORETICAL CALCULATIONS

To discuss the observed results concerning the collision energy dependence of the σ_{em}s for emission bands, the interaction potentials for a He*($2\,^3S$) atom approaching the sulphur atom in several directions were calculated for the entrance channel using *ab initio* molecular orbital methods.

For the He*($2\,^3S$)+$H_2S(\tilde{X}\,^1A_1)$ system as the entrance channel, there are difficulties associated with calculating the excited states embedded in an ionization continuum. A Li($2\,^2S$) atom was therefore used in place of He*($2\,^3S$) in the present study due to the well-known resemblance between He*($2\,^3S$) and Li($2\,^2S$) in interaction with various atomic targets.[12] Recently, Li model potentials were successfully applied to polyatomic targets in reproducing the collision energy dependence of partial Penning ionization cross sections.[13] The interaction potentials between a Li($2\,^2S$) atom and $H_2S(\tilde{X}\,^1A_1)$ were calculated using the GAUSSIAN 98 program package[14] both by the Møller–Plesset perturbation method (MP2) with a frozen-core approximation and by the density functional method (B3LYP). The standard 6-31++G($3df$,$3pd$) basis set was used. All calculations were performed with personal computers.

IV. RESULTS AND DISCUSSION

A. Potential energy surfaces for the entrance channel

Figure 1 shows the potential curves $V^*(R)$ for the $H_2S(\tilde{X}\,^1A_1)$+Li($2\,^2S$) system as the entrance channel obtained from the model potential by the MP2 calculation when the Li atom approaches along a plane perpendicular to the molecular plane; R is the distance between the Li atom and the S atom when the Li atom approaches from several directions, and θ represents the angle between the R(Li–S) vector and the C_2 axis. When the Li atom approaches from either the head or the tail side along the molecular axis, the V^* shows a shallow dip of 10 meV and is nearly repulsive. In contrast, when the Li atom approaches with $\theta = 90°$ in the plane perpendicular to the molecular plane, the V^* shows a deep well of 100 meV around $R = 0.27$ nm; the depth is 120 meV in the B3LYP calculation. This attractive tendency originates in the lone pair orbital. In contrast, when the Li atom approaches in the molecular plane, the V^* is nearly isotropic and has a shallow dip of 10 meV in $\theta = 0° - 180°$. Therefore the V^* around the molecular axis appears to be very anisotropic.

B. Emission spectra and emission cross sections

Figure 2 shows the emission spectrum observed at $E_R = 150$ meV. The hydrogen Balmer lines H($n = 3-8 \rightarrow 2$) and

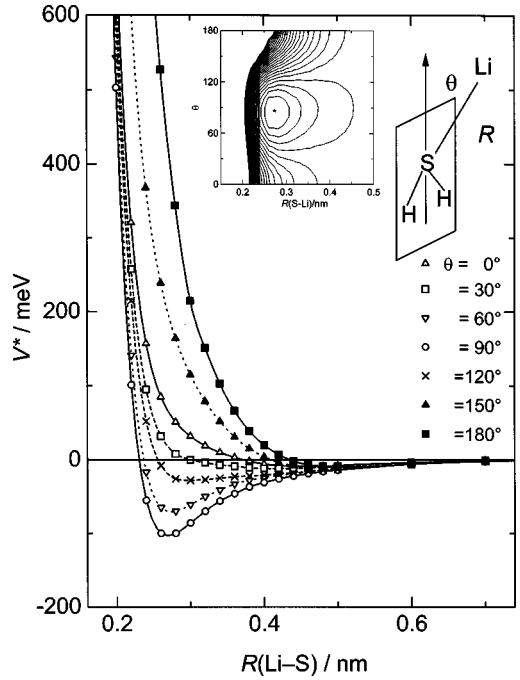

FIG. 1. Model potential curves $V^*(R)$ for $H_2S(\tilde{X}\,^1A_1)+Li(2\,^2S)$ as a function of the Li–S distance; θ represents the angle between the molecular axis and the Li–S vector when the Li atom is in the plane perpendicular to the molecular plane. The asterisk (*) in the contour map shows the minimum.

the 1–0, 0–0, 0–1, and 0–2 bands of the $SH^+(A\,^3\Pi-X\,^3\Sigma^-)$ emission were assigned. We did not identify any emission from $\nu' \geqslant 2$ of $SH^+(A\,^3\Pi)$. This result is consistent with the observation and discussion by Horani *et al.*[15] and Rostas *et al.*[16] Moreover, the strong bending progressions of the $H_2S^+(\tilde{A}\,^2A_1-\tilde{X}\,^2B_1)$ emission were assigned for the first time in the spectrum produced by the Penning ionization. In the assignment of the vibrational bands, we applied both the published data[17,18] and the calculated energies for the vibrational states, which are described in Paper I.

H_2S is an 18-electron system, and the electronic configuration of the ground state for the valence is

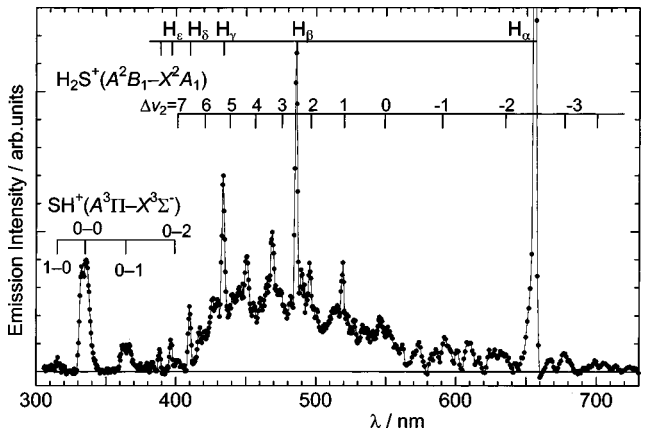

FIG. 2. Emission spectra produced by the collision of $He^*(2\,^3S)$ with H_2S at the $E_R=150$ meV with the 2 nm full width half maximum (FWHM) resolution.

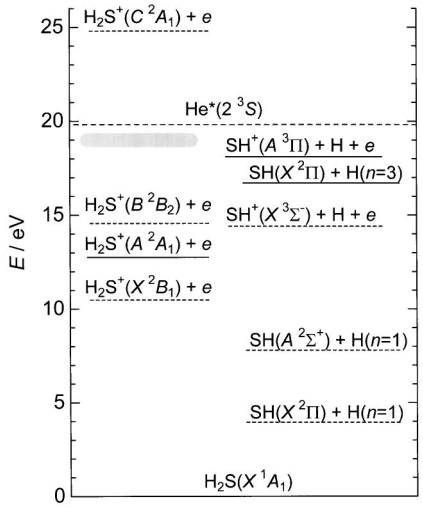

FIG. 3. Energy-level diagram for H_2S and related states; the solid lines mean the states found in this study. See the text for further information.

$$(4a_1)^2(2b_2)^2(5a_1)^2(2b_1)^2.$$

The four lowest H_2S^+ ion states come out of the four highest occupied orbitals. Figure 3 shows the energy-level diagram for H_2S, its ions, and energetically possible dissociation products. For the energies of these states we adopted the adiabatic ionization potentials,[19–21] the enthalpies of formation,[22] and the electronic energies of related species.[15,17,23] The ionization potential of $H_2S^+(\tilde{C}\,^2A_1)$ is estimated to be 22–26 eV.[24,25] The broad gray line represents possible precursor states correlating with the product $SH^+(A\,^3\Pi)+H+e$. The photoabsorption spectrum of H_2S shows a continuous band in the 15–20 eV range with very weak peaks at 18.5 and 19.8 eV, which were assigned to the quartet states of H_2S^+.[26] Nevertheless, the probability of producing the quartet state would be quite small in the Penning ionization because of a two-electron excitation. The $H_2S^+(\tilde{B}\,^2B_2)$ state is known to dissociate into the $SH^+(X\,^3\Sigma^-,\ ^1\Delta,\ \text{or}\ ^1\Sigma^+)+H+e$ product.[27–29] Therefore, the $(4a_1)^{-1}nl$ Rydberg states are the most probable candidate, and the $SH^+(A)+H+e$ state then seems to be produced via predissociation.

Table I summarizes the σ_{em} values obtained for the spe-

TABLE I. Emission cross sections σ_{em} obtained at a collision energy of 150 meV.

Species	λ/nm[a]	$\sigma_{em}/10^{-22}$ m^{2}[b]
1–0 band of $SH^+(A-X)$	310.4–327.2	0.8 (0.2)
0–0 band of $SH^+(A-X)$	328.3–345.8	10.3 (1.7)
0–1 band of $SH^+(A-X)$	357.3–374.8	2.9 (0.6)
H(7–2)	394.3–398.8	0.7 (0.2)
H(6–2)	407.8–412.3	1.6 (0.3)
H(5–2)	431.8–436.3	3.3 (0.7)
H(4–2)	483.3–487.8	6.1 (1.2)
H(3–2)	651.8–658.8	14.4 (3.1)
$H_2S^+(\tilde{A}-\tilde{X})$	400–700	129 (22)
Total	200–700	170 (30)

[a]The wavelength range for the measurement.
[b]The number in parentheses represents the experimental error.

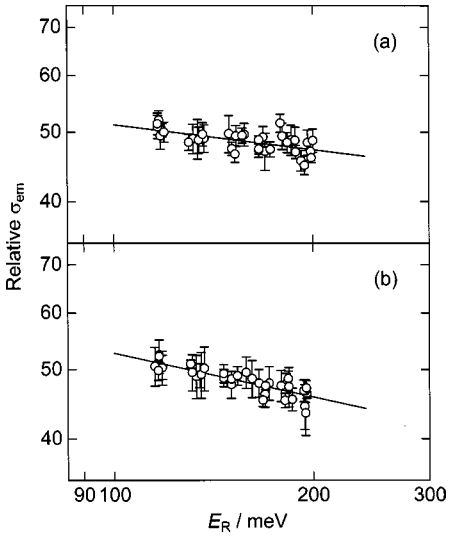

FIG. 4. $\log(\sigma_{em})$ vs $\log(E_R)$ plots for (a) the $SH^+(A-X)$ band and (b) the $H_2S^+(\tilde{A}-\tilde{X})$ band.

cies measured in the 200–700 nm region at E_R of 150 meV. Although the $H_2S^+(\tilde{A}-\tilde{X})$ emission was detected at a wavelength longer than 700 nm, we did not include it in the σ_{em} value because of the large uncertainty in the calibration of the photon-detecting system. The contribution from the wavelength longer than 700 nm was roughly estimated to be 10% of the $H_2S^+(\tilde{A}-\tilde{X})$ emission. Total σ_{em} in the 200–700 nm region was evaluated to be $(1.7\pm0.3)\times10^{-20}$ m^2.

To investigate the mechanism for formation of excited states, we measured the dependence of the σ_{em} value on the collision energy. If the attractive part of the interaction potential $V^*(R)$ between He*(2 ^3S) and H_2S is described by

$$V^*(R) = -C_S/R^{-S}, \tag{3}$$

the cross section is represented by[30]

$$\sigma(E_R) \propto E_R^{-2/s}. \tag{4}$$

When the collision energy is very low, the cross section for the Penning ionization decreases with increasing collision energy, eventually reaching a minimum.[31] As the collision energy is further increased, the cross section reaches a maximum and then decreases again at higher energies. Under the orbiting approximation, this result can be applied to the formation of fragment ions if the branching ratio among possible decay channels does not depend on the collision energy.

In this study, the kinetic energy dependence of the σ_{em} value was measured at 336.5 nm for the 0–0 band of the $SH^+(A\,^3\Pi-X\,^3\Sigma^-)$ system and at 451 nm for the (0, 4, 0–0, 0, 0) band of the $H_2S^+(\tilde{A}\,^2A_1-\tilde{X}\,^2B_1)$ system. Figure 4 shows the dependences for the $SH^+(A-X)$ and $H_2S^+(\tilde{A}-\tilde{X})$ bands. Both emissions were found to decrease with increasing E_R; the s value estimated from the slopes is 17 for the $SH^+(A-X)$ band and 10 for the $H_2S^+(\tilde{A}-\tilde{X})$ band. This result indicates that either an attractive potential governs formation of the emitters, or that the collision reaches the high speed limit. The V^* surface shows a deep well of 100 meV in the direction perpendicular to the molecular plane. Therefore, we believe it likely that the effective potential is attractive for formation of $SH^+(A)$ and $H_2S^+(\tilde{A})$. The geometrical arrangement where the He*(2 ^3S) atom is in the direction perpendicular to the molecular plane seems to be effective for formation of these ions. The relative smallness of the slope for the $SH^+(A-X)$ band probably originates in the precursor state being produced by the excitation of an electron from an orbital closer to the nucleus than the $5a_1$ orbital for forming $H_2S^+(\tilde{A}\,^2A_1)$, although the precursor is not identified. The precursor state for $SH^+(A)$ will be produced at relatively small R, where the effective potential shows a more repulsive character, and the slope for the $SH^+(A-X)$ band will then become smaller.

C. Rotational distribution of the $SH^+(A-X)$ system

In the $SH^+(A\,^3\Pi-X\,^3\Sigma^-)$ emission, the 1–0 band is far weaker than the 0–0 and 0–1 bands because of predissociation.[16,32] We therefore apply the band-envelope analysis only to the 0–0 band.

If the radiationless processes do not occur within the lifetime, the population of a rotational state N' of the $SH^+(A\,^3\Pi,\ \nu'=0)$ state is proportional to its photoemission intensity. The emission intensity of a transition from the N' state to an N'' state is represented by

$$I_{N'N''} \propto \varepsilon_{N'N''}(\nu_{N'N''})^3 S_{N'N''} P(N')/(2N'+1), \tag{5}$$

where ε is the efficiency of the photon-detection system, ν is the transition frequency, S is the rotational line strength, and $P(N')$ is the formation rate of the N' state. There are 27 branches in the $A\,^3\Pi_{(a)}-X\,^3\Sigma^-$ system, and the transition from Hund's coupling case (a) to (b) is very slow with increasing N'.[15] The line strengths were calculated by the formulas described by Schadee.[33] The $^NP_{13}$ and $^TR_{31}$ branches with particularly small line strengths were neglected in the band-envelope analysis. The transition frequencies of the 0–0 band, which were calculated by using the formulas and the molecular constants given by Rostas *et al.*,[16] agree with the observed values within 0.2 cm^{-1}.

Figure 5 shows the Fortrat diagram for 25 branches and the observed spectrum compared with the synthetic spectrum. In the analysis, the population for the N' level is assumed as the same among the $^3\Pi_0$, $^3\Pi_1$, and $^3\Pi_2$ components, despite the large spin–orbit splitting. The agreement between the observed and synthetic spectrum is very good except in the 331–333 nm region. The discrepancy around 332 nm may be due to several causes such as (1) overlapping with another emission, (2) the enhancement in the population for the $^3\Pi_2$ component, and (3) the enlargement in the $S_{N'N''}$ for the $^3\Pi_2$ component. The $N_2^+(B-X)$ band from background gas or the $H_2S^+(\tilde{A}\,^2A_1-\tilde{X}\,^2B_1)$ band could possibly overlap around 332 nm. Nevertheless, we believe it unlikely that these bands overlap based on both the transition frequencies and the FCFs. The anomaly in either the population or the $S_{N'N''}$ values for the $^3\Pi_2$ component may be caused by perturbation with the $a\,^1\Delta$ and/or $^5\Sigma^-$ states.[16] The a state is estimated to be 2.5 eV lower than the $^3\Pi_2$ state,[15] while would then lessen the perturbation. The production of a high spin state such as that of a quintet has not yet been reported

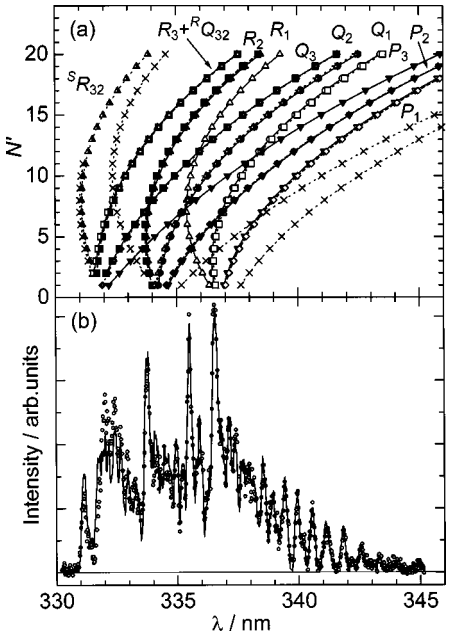

FIG. 5. Transition for the $SH^+(A\,^3\Pi - X\,^3\Sigma^-)$ system: (a) Fortrat diagram on N' for 25 branches, (b) the observed spectrum (circle) compared with the synthetic spectrum (solid curve) with the 0.2 nm FWHM resolution.

in the collision of He*$(2\,^3S)$ with simple molecules. Enhancement of the $^3\Pi_2$ component therefore does not seem to occur by perturbation with other states. We believe it likely that the $S_{N'N''}$ values for the $^3\Pi_2$ state are enlarged due to perturbation, since the artificial analysis with twice the $S_{N'N''}$ values for the R_3 and $^RQ_{32}$ branches shows much better agreement with the observed spectrum. Nevertheless, rotational populations obtained by using several sets altered artificially around the $S_{N'N''}$ values for the $^3\Pi_2$ state were found to be nearly constant. We therefore concluded that the rotational populations for the $SH^+(A\,^3\Pi,\ v'=0)$ state are independent of the discrepancy around 332 nm. Figure 6 shows the populations up to $N'=17$ normalized by the multiplicity $\log[P(N')/(2N'+1)]$ as a function of $N'(N'+1)$. The date were fitted by a straight line, and the rotational temperature of 870 ± 80 K obtained from the slope is constant in $E_R=115-200$ meV. The populations for $N'\geqslant 18$ decrease suddenly and then disappear due to predissociation.[16]

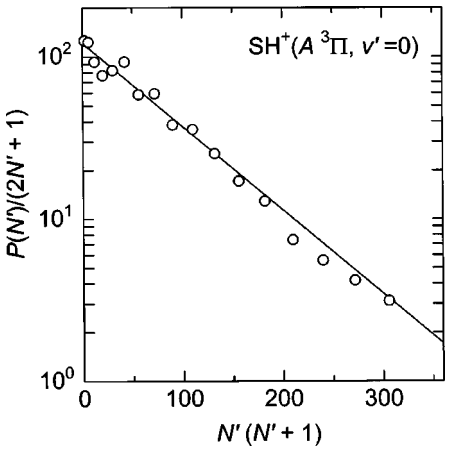

FIG. 6. Rotational populations of $SH^+(A\,^3\Pi, v'=0)$. The sold line represents a rotational temperature of 870 K.

The precursor state for formation of $SH^+(A\,^3\Pi)$ is probably Rydberg states correlating with the $H_2S^+(\tilde{C}\,^2A_1)$ state, as discussed in a previous section. From the Walsh diagram, the H–S–H angle of $H_2S^+(\tilde{C})$ is considered to be smaller than that of $H_2S(\tilde{X})$ in equilibrium. Narrowing of the H–S–H angle would therefore follow due to the transition to the Rydberg states. By this dynamical effect, the $SH^+(A\,^3\Pi)+H+e$ product gains torque, which may rotationally excite the $SH^+(A\,^3\Pi)$ state. Nevertheless, the observed temperature is not particularly high. We may therefore conclude that the potential surface for predissociation is a late barrier type.

D. Vibrational distribution of the $H_2S^+(\tilde{A}-\tilde{X})$ system

In the preliminary analysis of the $H_2S^+(\tilde{A}-\tilde{X})$ spectra, the bending (ν_2) progressions are found to be prominent. Populations for the $(\nu_1'=1$ or 2, ν_2', $\nu_3'=0)$ combination states of $H_2S^+(\tilde{A})$, which have moderate FCFs for the $H_2S(\tilde{X})\rightarrow H_2S^+(\tilde{A})$ ionization, are therefore neglected. H_2S^+ is an asymmetric top molecule, and the rotational energies of the $\tilde{X}\,^2B_1$ and $\tilde{A}\,^2A_1$ states are represented by three quantum numbers, N, K_a, and K_c.[34] The rotational and vibrational energies for the $(\nu_1'=0, \nu_2', \nu_3'=0)$ level of $H_2S^+(\tilde{A})$ and the $(\nu_1'', \nu_2'', \nu_3'')$ level of $H_2S^+(\tilde{X})$ were calculated by the formulas and the constants reported by Duxbury *et al.*[18] The rotational constants for higher vibrational levels are extrapolated from their data. The vibrational energies are calculated for both higher bending modes and combination modes, as described in Paper I.

In the population analysis of $H_2S^+(\tilde{A})$, we assumed that the rotational distribution for each vibrational state to be represented by a Boltzmann temperature because of low spectral resolution. If the radiationless processes do not occur within the lifetime, the population of a $(\nu_1'=0, \nu_2', \nu_3'=0, N', K_a', K_c')$ state is proportional to its photoemission intensity. Therefore, the emission intensity of a transition from the $m(0, \nu_2', 0, N', K_a', K_c')$ state to an $n(\nu_1'', \nu_2'', \nu_3'', N'', K_a'', K_c'')$ state can be represented by

$$I_{mn}\propto \varepsilon_{mn}A_{mn}P(\nu_2')S_{mn}\exp\left[-\frac{E_m}{RT_m}\right], \tag{6}$$

where A_{mn} is Einstein's A coefficient for the spontaneous emission except the rotational transition, $P(\nu_2')$ is the formation rate for the $(0, \nu_2', 0)$ level, E_m is the rotational energy, and T_m is the rotational temperature. Einstein's A coefficients were calculated in this study as described in Paper I. As for the Hönl–London factor we approximated the formulas of the vertical band for the symmetric top.[34]

The $(0, \nu_2'=0-10, 0)$ levels were selected as the emitting state, and the 95 bands with large A coefficients were included in the band-envelope analysis. Figure 7 shows the synthetic spectra comparing with the observed spectra. We tried several sets of the rotational temperatures for $\nu_2'=0-10$, and these temperatures are estimated to be 800–1200 K. The synthetic spectrum agrees modestly with the

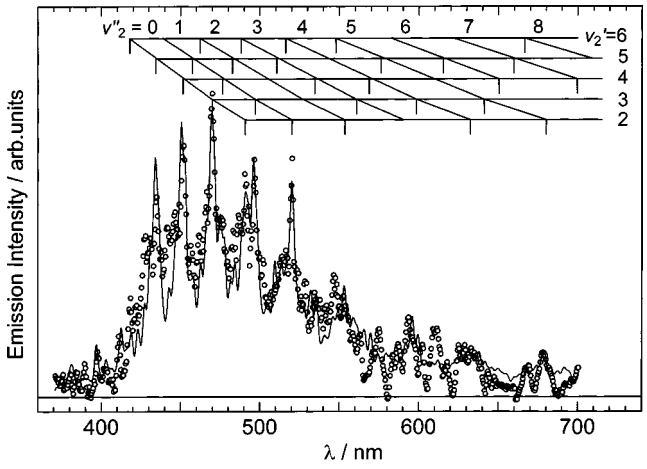

FIG. 7. The observed spectrum (○) of the $H_2S^+(\tilde{A}\,^2A_1-\tilde{X}\,^2B_1)$ transition is compared with the synthetic spectrum (solid curve).

observed spectrum. The discrepancy is probably caused primarily by the vibrational energies calculated for the higher bending states that probably deviate from the true values. Moreover the combination states that borrowed their intensities from the pure bending levels seem to appear, since several anharmonic constants for $H_2S^+(\tilde{A}\,^2A_1)$ are very large and the coupling therefore seems to become large. Figure 8 plots the vibrational distribution observed for the $(0, \nu_2'' = 0-10, 0)$ levels comparing with the FCFs calculated for the $(0,0,0)\rightarrow(0, \nu_2', 0)$ bands of the $H_2S(\tilde{X}\,^1A_1) \rightarrow H_2S^+(\tilde{A}\,^2A_1)$ ionization in this study; the details are described in Paper I. The observed distribution has a peak at $\nu_2'=3$ and is shifted to lower ν_2' than that predicted by the FCFs with a peak at $\nu_2'=6-7$. The photoelectron spectrum (PES) of H_2S shows a peak at $\nu_2'=4-5$, which is considered to be a Franck–Condon (FC) type.[17,35] The peak in the theoretical FCF is shifted higher than that observed from PES, probably due to neglect of the dependence of the electronic transition moment on the vibrational states. The maximum in Einstein's B coefficients, which incorporate the dependence of the transition probabilities on the vibrational states for the $H_2S(\tilde{X})\rightarrow H_2S^+(\tilde{A})$ ionization, is expected to shift to lower ν_2' since the transition moment is estimated to be larger around the equilibrium geometry from the analogy of the $H_2S^+(\tilde{X}-\tilde{A})$ transition.

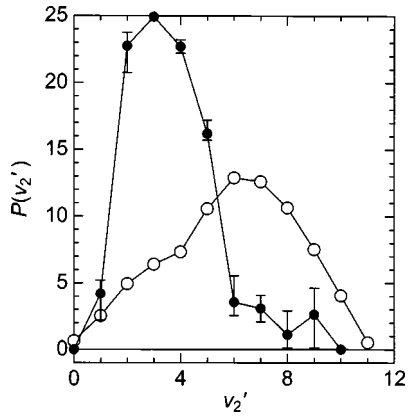

FIG. 8. Vibrational distribution for the $(0,\nu_2',0)$ level of the $H_2S^+(\tilde{A}\,^2A_1)$ state: the observed data (solid circle) is compared with the FCFs (open circle) calculated for the $H_2S(\tilde{X}\,^1A_1)\rightarrow H_2S^+(\tilde{A}\,^2A_1)$ ionization.

In order to study the ionization dynamics for formation of $H_2S^+(\tilde{A})$ by Penning ionization of H_2S, it is important to compare the vibrational distribution of $H_2S^+(\tilde{A})$ obtained from the $H_2S^+(\tilde{A}-\tilde{X})$ emission by PIOS with those by PIES; PIES gives information on the state immediately after ionization, while PIOS gives that the fluorescence lifetime later. The vibrational structure in the PIES of H_2S with He*(2 ^3S), which is partly resolved, shows features very similar to the PES measured under the same conditions.[36] Accordingly, we may conclude that the formation of $H_2S^+(\tilde{A})$ by He*(2 ^3S) Penning ionization is an FC type. The discrepancy between PIES and PIOS doubtlessly originates in either predissociation or vibrational coupling in the $\tilde{A}$ state. Even if the pure bending state is produced primarily, some combination states may be populated through vibrational energy transfer. The rate of the vibrational energy transfer depends on not only the vibrational state density but also the anharmonicity of the $\tilde{A}$ state.[37] This means combination states near the pure bending state may be populated since the anharmonicity constants are relatively large in the $\tilde{A}$ state. Nevertheless, no emission from the combination states near the pure bending states was assigned. We concluded that the vibrational energy transfer does not come up as serious problem.

The vibrational levels with $\nu_2'\geqslant 6$ of $H_2S^+(\tilde{A})$ are known to cause predissociation into the $S^+ + H_2$.[17,27,38] The sudden decrease in the population observed for $\nu_2'\geqslant 6$ appears to be caused by the predissociation. This effect is remarkable for the states with a higher vibrational quantum number. Although we cannot quantitatively estimate the effect by predissociation, we may still claim that the vibrational distribution of $H_2S^+(\tilde{A})$ is shifted to lower ν_2' than that of the FC type. In the calculation of FCFs for the $H_2S(\tilde{X})\rightarrow H_2S^+(\tilde{A})$ ionization, the $H_2S^+(\tilde{A})$ state is populated primarily in the pure bending mode $(0, \nu_2' = 2-10, 0)$. Even if the nascent distribution of $H_2S^+(\tilde{A}\,^2A_1)$ is an FC type, the pure bending state, especially higher states, probably dissipates to some extent into combination states that are coupled with the initial bending state within the radiative lifetime of 2–5 μs.[27,38] These coupling states either radiate with transition frequencies that are different from that for the initial bending state or do not radiate. Therefore, the vibrational distribution obtained from the $H_2S^+(\tilde{A}-\tilde{X})$ emission deviates from the nascent distribution. The broadening of the peak for each vibrational sequence seems to be caused partly by the emissions from combination states. Nevertheless, we did not identify any band from combination states. Even if any emissions from combination states did occur, they would be hidden by intense bending progressions.

V. CONCLUSION

The mechanism of formation of excited states by the collision of He*(2 ^3S) with H_2S was studied by optical spec-

troscopy. The $H_2S^+(\tilde{A}\,^2A_1-\tilde{X}\,^2B_1)$ emission was observed in the collision of $He^*(2\,^3S)$ with H_2S for the first time. The analysis of the $H_2S^+(\tilde{A}-\tilde{X})$ system showed that the $H_2S^+(\tilde{A})$ state is populated only in the pure bending mode $(0, \nu_2'=2-8, 0)$. The observed distribution with a peak around $\nu_2'=3$ is shifted lower than the distribution with a peak around $\nu_2'=6-7$ predicted from FCF, and that with a peak around $\nu_2'=4-5$ observed from PES and PIES. This discrepancy is caused not only by the predissociation above $\nu_2' \geqslant 6$, but also by the intensity borrowing by combination states, which may be coupled with the pure bending state.

The rotational distribution of the $SH^+(A\,^3\Pi,\ \nu'=0)$ state is represented by a Boltzmann temperature of 870 ± 80 K, which is nearly constant in the $E_R=115-200$ meV range. The precursor state for formation of $SH^+(A\,^3\Pi)$ is probably Rydberg states correlating with $H_2S^+(\tilde{C}\,^2A_1)$, and the $SH^+(A\,^3\Pi)+H+e$ state is then produced by predissociation. $SH^+(A)$ is expected to be rotationally hot based on consideration of the Walsh diagram. The fact that the observed temperature is not particularly high leads us to assume that the potential surface for predissociation would be a late barrier type.

ACKNOWLEDGMENTS

This work was supported by Grant-in-Aid from the Ministry of Education, Science, and Culture (Grant Nos. 11640499 and 13740336) and by the Joint Research Program of IMS. I.T. greatly appreciates Professor K. Ohno for providing the unpublished data and also thanks the Uchida Science Foundation.

[1] V. Čermák and A. J. Yencha, J. Electron Spectrosc. Relat. Phenom. **11**, 67 (1977).
[2] C. E. Brion and D. S. C. Lee, J. Electron Spectrosc. Relat. Phenom. **12**, 77 (1977).
[3] K. Mitsuke, T. Takami, and K. Ohno, J. Chem. Phys. **91**, 1618 (1989).
[4] M. Tsuji, K. Tsuji, H. Fukutome, and Y. Nishimura, Chem. Lett. **1977**, 673.
[5] A. J. Yencha and K. T. Wu, Chem. Phys. **32**, 247 (1978).
[6] M. Tsuji, J. P. Maier, H. Obase, and Y. Nishimura, Chem. Phys. Lett. **147**, 619 (1988).
[7] I. Tokue, I. Kudo, and Y. Ito, Chem. Phys. Lett. **199**, 435 (1992).
[8] I. Tokue, Y. Sakai, and K. Yamasaki, J. Chem. Phys. **106**, 4491 (1997).
[9] K. Ohno, T. Takami, K. Mitsuke, and T. Ishida, J. Chem. Phys. **94**, 2675 (1991) and references cited therein.
[10] R. A. Sanders, A. N. Schweid, M. Weiss, and E. E. Muschlitz, Jr., J. Chem. Phys. **65**, 2700 (1976).
[11] F. J. Comes and F. Speier, Chem. Phys. Lett. **4**, 13 (1969).
[12] (a) H. Haberland, Y. T. Lee, and P. E. Siska, Adv. Chem. Phys. **45**, 487 (1981); (b) H. Hotop, T. E. Roth, M.-W. Ruf, and A. J. Yencha, Theor. Chem. Acc. **100**, 36 (1998).
[13] (a)T. Pasinszki, N. Kishimoto, and K. Ohno, J. Phys. Chem. A **103**, 6746 (1999); (b) N. Kishimoto, Y. Osada, and K. Ohno, *ibid.* **104**, 1393 (2000).
[14] M. J. Frisch, G. W. Trucks, H. B. Schlegel *et al.*, GAUSSIAN 94, Revision B.2, Gaussian, Inc., Pittsburgh, PA, 1995.
[15] M. Horani, J. Rostas, and H. Lefebvre-Brion, Can. J. Phys. **45**, 3319 (1967).
[16] J. Rostas, M. Horani, J. Brion, D. Daumont, and J. Malicet, Mol. Phys. **52**, 1431 (1984).
[17] R. N. Dixon, G. Duxbury, M. Horani, and J. Rostas, Mol. Phys. **22**, 977 (1971).
[18] G. Duxbury, M. Horani, and J. Rostas, Proc. R. Soc. London, Ser. A **331**, 109 (1972).
[19] D. W. Turner, C. Baker, A. D. Baker, and C. R. Brundle, *Molecular Photoelectron Spectroscopy* (Wiley-Interscience, New York, 1970).
[20] (a) J. Delwiche, P. Natalis, and J. E. Collins, Int. J. Mass Spectrom. Ion Phys. **5**, 443 (1970); (b) J. Delwiche and P. Natalis, Chem. Phys. Lett. **5**, 564 (1970).
[21] A. W. Potts and W. C. Price, Proc. R. Soc. London, Ser. A **326**, 181 (1972).
[22] D. D. Wagman, W. H. Evans, V. B. Parker, R. H. Schumm, I. Halow, S. M. Bailey, K. L. Churney, and R. L. Nuttall, J. Phys. Chem. Ref. Data **11**, 2 (1982).
[23] K. P. Huber and G. Herzberg, *Molecular Spectra and Molecular Structure*, Constants of Diatomic Molecules, Vol. 4 (Van Nostrand Reinhold, New York, 1979).
[24] D. M. Chapman, J. Electron Spectrosc. Relat. Phenom. **14**, 323 (1978).
[25] W. Domcke, L. S. Cederbaum, J. Schirmer, W. von Niessen, and J. P. Maier, J. Electron Spectrosc. Relat. Phenom. **14**, 59 (1978).
[26] T. Ibuki *et al.*, Chem. Phys. Lett. **119**, 327 (1985).
[27] J. H. D. Eland, Int. J. Mass Spectrom. Ion Phys. **31**, 161 (1979).
[28] H. F. Prest, W.-B. Tzeng, J. M. Brom, Jr., and C. Y. Ng, Int. J. Mass Spectrom. Ion Phys. **50**, 315 (1983).
[29] G. Hirsch and P. J. Bruna, Int. J. Mass Spectrosc. Ion Phys. **36**, 37 (1980).
[30] A. Niehaus, Adv. Chem. Phys. **45**, 399 (1981) and references cited therein.
[31] R. E. Olson, Phys. Rev. A **6**, 1031 (1972).
[32] C. P. Edwards, C. S. Maclean, and P. J. Sarre, Mol. Phys. **52**, 1453 (1984).
[33] A. Schadee, Astron. Astrophys. **41**, 213 (1975).
[34] G. Herzberg, *Molecular Spectra and Molecular Structure*, Infrared and Raman Spectra of Polyatomic Molecules, Vol. 2 (Van Nostrand, Princeton, 1945).
[35] L. Karlsson, L. Mattsson, R. Jardny, T. Bergmark, and K. Siegbahn, Phys. Scr. **12**, 229 (1976).
[36] K. Ohno (private communication).
[37] K. A. Holbrook, M. J. Pilling, and S. H. Robertson, *Unimolecular Reactions*, 2nd ed. (Wiley, Chichester, 1996).
[38] G. R. Möhlmann and F. J. de Heer, Chem. Phys. Lett. **36**, 353 (1975).